Title: AKAP350 regulates cytoskeleton remodeling and LFA-1 organization during NK cytolytic response

Authors: Alejandro P. Pariani[1], Evangelina Almada[1], Florencia Hidalgo[1], Carla Borini-Etichetti[1], Rodrigo Vena[2], Cristián Favre[1], James R. Goldenring[3], M. Cecilia Larocca[1]*

Affiliation: [1]Instituto de Fisiología Experimental, Consejo Nacional de Investigaciones Científicas y Técnicas (CONICET), Facultad de Ciencias Bioquímicas y Farmacéuticas, Universidad Nacional de Rosario (UNR), (2000) Rosario, Argentina.

[2] Instituto de Biología Molecular y Celular de Rosario, CONICET, Facultad de Ciencias Bioquímicas y Farmacéuticas, UNR, Rosario, Argentina.

[3] Epithelial Biology Center and Department of Cell & Developmental Biology, Vanderbilt University School of Medicine, Nashville, Tennessee, USA

Corresponding Author's Information: M. Cecilia Larocca, Instituto de Fisiología Experimental, Facultad de Ciencias Bioquímicas y Farmacéuticas. Suipacha 570, 2000 Rosario, Argentina. Tel: 54-341-4305799. E-mail: larocca@ifise-conicet.go

Abstract

Natural killer (NK) cell cytotoxicity requires extensive cytoskeleton remodeling and receptors reorganization at the site of NK/target cell interaction (immune synapse, IS). How these processes are integrated remains unclear. We found that AKAP350, a scaffold protein that regulates microtubule dynamics, was required for NK cytolytic activity. Reduction of AKAP350 expression inhibited actin and LFA-1 reorganization and centrosome translocation to the IS. AKAP350KD cells showed decreased microtubule nucleation at the Golgi apparatus and reduced localization at the centrosome and at the IS of CIP4, an AKAP350 interacting protein that regulates centrosome translocation to the IS. AKAP350 delocalization from the Golgi or pharmacological disruption of microtubule dynamics or Golgi function impaired LFA-1 clustering at the IS, preserving actin remodeling. These data support a role for AKAP350 in the integration of actin and microtubule remodeling during NK activation and reveal for the first time the participation of the Golgi apparatus in NK-IS maturation.

16 **Introduction**

17 Natural killer cells (NK) are the cytolytic effectors of the innate immune system, which
18 constitute the first line of immunological defense and are particularly relevant for the
19 elimination of viral infected and neoplastic cells. NK cytotoxic effector function relies on
20 the formation of a specialized junction with its target cell, generally referred to as immune
21 synapse (IS). In the case of NK lytic IS, the persistent outside-in signaling generated by
22 the interaction of NK activating receptors with their ligands in a susceptible target cell,
23 in a context of absence of inhibitory signals, triggers a multistep, highly regulated process
24 that culminates with the directed secretion of lytic molecules contained in specialized
25 lysosomes (lytic granules) (Mace et al., 2014). An early event in this process is actin
26 cytoskeleton remodeling into an F-actin-rich supramolecular activation cluster (SMAC)
27 at the IS, and the subsequent clustering of cell-surface receptors at this site. IS maturation
28 requires actin organization as a compact mesh at the SMAC periphery and a less dense
29 net of branching filaments at the IS center (Brown et al., 2011), where lytic degranulation
30 takes place (Rak et al., 2011). Immediately after actin reorganization at the IS, the
31 centrosome, usually regarded as the main microtubule organizing center (MTOC) in NK
32 cells, translocates to the IS, enabling lytic granules translocation and directed secretion
33 of lytic granules contents into the target cell (Mace et al., 2014). Therefore, the
34 development of NK lytic response requires an extensive, synchronized actin and
35 microtubule remodeling. Even though some proteins that participate in actin and
36 microtubule dynamics during the NK lytic IS, such as WASP (Orange et al., 2002),
37 CDC42 (Carlin et al., 2011) and the CDC42 interacting protein 4 (CIP4) (Banerjee et al.,
38 2007) have been identified, the mechanisms that coordinate actin and microtubule
39 remodeling remain poorly understood.

40 The A-kinase anchoring protein 350 (AKAP350), also known as AKAP450, CG-NAP or
41 AKAP9, is a centrosome and Golgi apparatus-scaffold protein (Schmidt et al, 1999) that
42 arises as a putative candidate to regulate cytoskeleton remodeling during the development
43 of the NK lytic response. AKAP350 has a prominent role in microtubule nucleation
44 (Takahashi et al., 2002, Rivero et al., 2009, Kolobova et al., 2019). AKAP350 also
45 participates in mitotic spindle orientation (Almada et al., 2017) and in centrosome
46 translocation towards the leading edge in migratory cells (Tonucci et al., 2015).
47 AKAP350 participation in microtubule remodeling is related to its capacity to scaffold
48 specific proteins at the centrosome and at the Golgi apparatus, including the members of
49 the γ-TURC CGP2/3 (Takahashi et al 2002), the casein kinase δ (Sillibourne et al., 2002),
50 CIP4 (Larocca et al., 2004), the component of the dynein/dynactin complex p150 glued
51 (Kim et al., 2007) and the plus end binding protein 1 (EB1) (Almada el al., 2017). The
52 involvement of AKAP350 in microtubule reorganization in response to outside-in
53 signaling in immune cells was first revealed by studies in T cells (El Din El Homasany et
54 al., 2005). Those studies demonstrated that the interference with AKAP350 function at
55 the centrosome leads to inhibition of lymphocyte function-associated antigen-1 (LFA-1
56 or αLβ2 integrin; CD11a/CD18) induced-cell migration. Later studies indicated that,
57 during antigen recognition by T-cells, AKAP350 participates in LFA-1 conformational
58 activation and centrosome translocation towards the IS (Robles Valero et al., 2010).
59 Regarding the mechanisms involved, they have not been elucidated.

60 In the present study we analyzed AKAP350 participation in the development of NK
61 cytotoxic effector function and characterized its role in actin and microtubule
62 cytoskeleton remodeling, and in LFA-1 reorganization at the lytic IS. We further
63 characterized microtubule nucleation in activated NK cells and evaluated the role of Golgi
64 associated AKAP350 in NK-IS maturation.

65 **Results**

66 1. AKAP350 localization at the Golgi apparatus in NK/YTS cells is up-regulated during
67 cell activation

68 To determine if AKAP350 could have a role in NK cytotoxic response, we first evaluated
69 its expression in YTS immortalized NK cells. Western blot analysis of YTS cell-extracts
70 indicates that AKAP350 is expressed in YTS cells. Immunofluorescence analysis of
71 AKAP350 staining in resting YTS cells showed that AKAP350 colocalized with γ-tubulin
72 and GM-130, what is indicative of AKAP350 localization at the centrosome and at the
73 Golgi apparatus (Figure 1A, B first row). KT86 cells are derived from K562
74 erythroleukemia cells and constitute susceptible targets for YTS cells. The analysis of
75 YTS:KT86 conjugates indicates that AKAP350 localization at the centrosome was
76 reduced (-50%), whereas its localization at the Golgi apparatus was increased (+44%) in
77 activated NK cells (Figure 1A, B, second row and bars). These results indicate that
78 activation of YTS cells induces a partial translocation of AKAP350 from the centrosome
79 to the Golgi apparatus.

80 2. Decrease of endogenous AKAP350 expression impairs NK cytolytic activity

81 To analyze the impact of AKAP350 expression in the development of NK cytolytic
82 effector function, we generated YTS cells with decreased AKAP350 expression
83 (AKAP350KD) using a lentiviral short hairpin RNA expression system targeting two
84 different AKAP350 mRNA sequences, as we have previously described (Tonucci et al.,
85 2015). Western blot analysis of AKAP350 protein levels showed that the expression of
86 either shRNA1 or shRNA4 efficiently decreased AKAP350 levels to less than 10% of

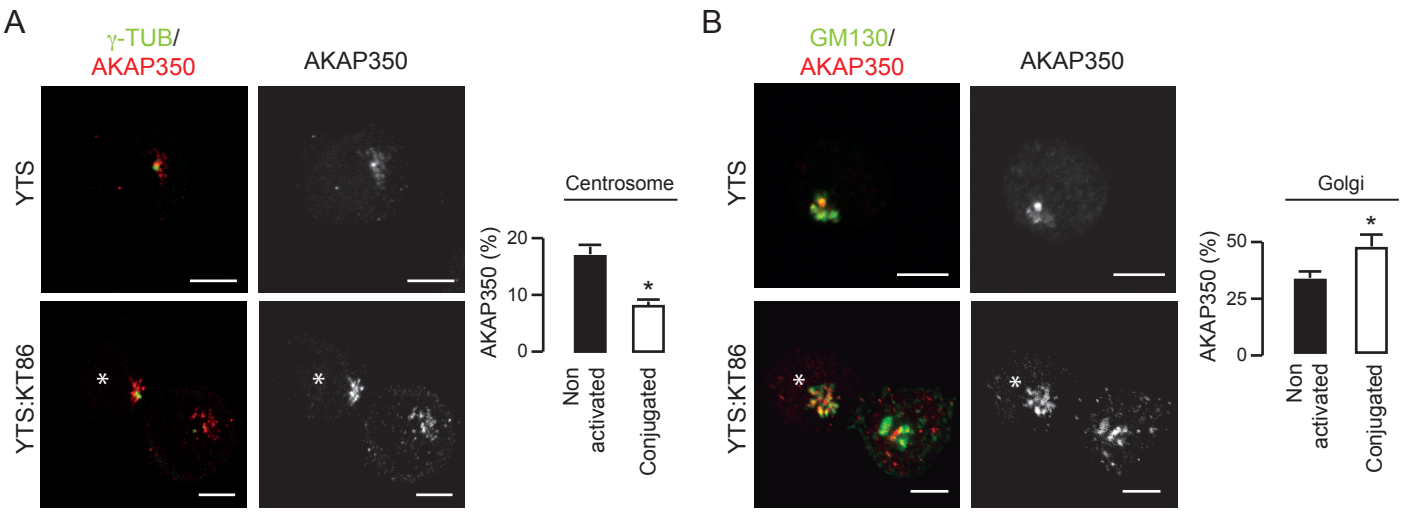

Figure 1. AKAP350 localization in YTS cells. Isolated YTS cells or YTS:KT86 conjugates were stained and analyzed by confocal microscopy (see Materials and methods). Merge images show YTS cells (upper row) or YTS:KT86 conjugates (lower row) staining for AKAP350 (red) and γ-tubulin (A) or GM130 (B) (green). Asterisk denotes YTS cells in YTS:KT86 conjugates. Bars represent the mean fraction of AKAP350 fluorescence present at centrosomes (A) or at the Golgi apparatus (B) in isolated or conjugated YTS cells, expressed as percentage of total AKAP350-fluorescence, representative of three independent experiments. At least 20 cells were analyzed for each experiment. Error bars represent SEM. *$p < 0.05$. Scale bars, 5 μm.

control levels (Figure 2A). To assess AKAP350 participation in NK adhesion to target cells, control and AKAP350KD YTS cells were labeled with TrackerTM Deep Red and KT86 cells were labeled with CFSE. Cells were incubated at different NK:target cell ratios, for different periods, and the formation of cell conjugates positive for both fluorophores was analyzed by FACS (Supplementary Figure 1). Our results showed that the decrease in AKAP350 expression did not elicit any evident effect in the initial adherence between NK and their susceptible target cells. In order to analyze NK cytolytic activity, control and AKAP350KD YTS cells generated by expression of shRNA1 or shRNA4 were incubated with CFSE-labeled KT86 cells at different NK:target cell ratios and target cell lysis was analyzed by FACS analysis of propidium iodide stained cells. Our results showed that the decrease in AKAP350 levels by expression of either shRNA1 or shRNA4 impaired NK cytolytic activity (Figure 2B,C).

3. AKAP350 participates in centrosome translocation towards the lytic IS

Our previous studies demonstrated that AKAP350 regulates centrosome translocation towards the leading edge in migratory cells, a process with some homology to the development of the IS. Considering that centrosome translocation to the IS is a critical step in NK cytolytic response, centrosome localization in control and AKAP350KD YTS cells conjugated with KT86 target cells was evaluated by confocal microscopy. To discriminate NK from target cells, KT86 cells were preloaded with CFSE. γ-tubulin staining was used to identify the centrosome, and the IS was defined as the region of YTS/KT86 contact delimited in the DIC channel. Centrosome translocation was impaired in YTS cells with decreased expression of AKAP350, as denoted by the greater distance between the MTOC and the centroid of the IS region in AKAP350KD cells ((Figure 3A). In non cytolytic T cells, AKAP350 participates in LFA-1 activation and the subsequent translocation of the centrosome to the IS (Robles Valero et al, 2010). Considering that

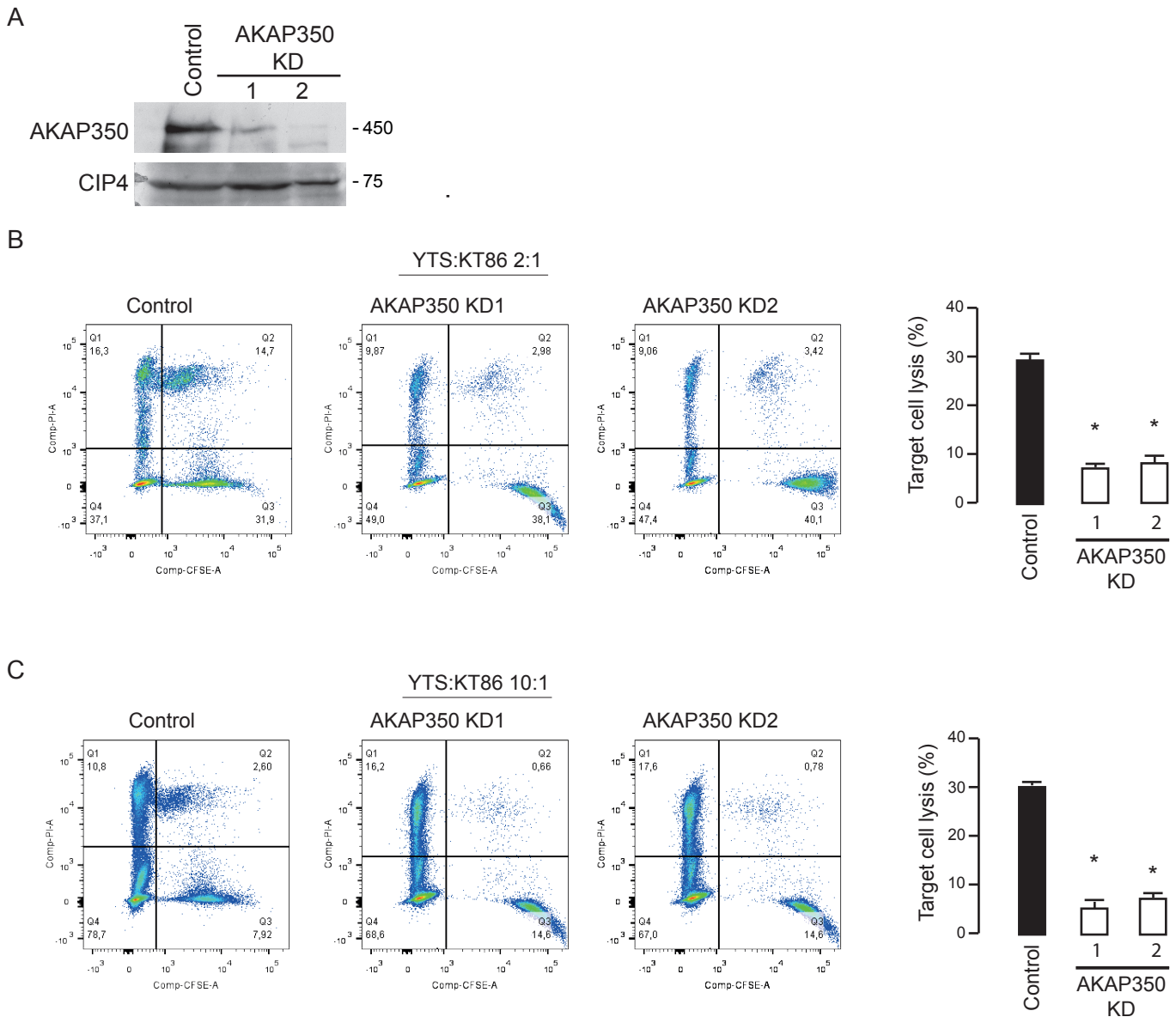

Figure 2. Reduction of AKAP350 expression levels diminishes YTS cells' cytotoxicity. Two different specific shRNAs (shRNA1 and shRNA4) were used to generate YTS cells with decreased AKAP350 expression (AKAP350KD1 and AKAP350KD2, respectively), as described in Materials and methods. A) Western blot analysis of AKAP350 expression in control, AKAP350KD1 and AKAP350KD2 YTS cells. CIP4 was used as loading control. B,C) KT86 cells were stained with CFSE and mixed with YTS cells at 2:1 (B) or 10:1 (C) effector: target ratios. After the incubation period, cells were stained with PI and analyzed by flow cytometry. YTS cytotoxic activity was estimated as the fraction of total CFSE positive events that were also positive for PI. Bars chart represents the mean percentage of double positive events for control, AKAP350KD1 and AKAP350KD2 cells, representative of three independent experiments. Error bars represent SEM. *$p < 0.05$.

112 LFA-1 activation is sufficient to induce MTOC translocation in NK cells, we analyzed
113 AKAP350 role in MTOC translocation upon specific activation of LFA-1 or CD28, an
114 additional NK receptor that induces MTOC translocation as well (Chen et al., 2006). YTS
115 cells activated on slides coated with ICAM-1 or with an activating anti-CD28 antibody
116 were stained and analyzed by confocal microscopy (Figure 3B,C). In both conditions,
117 AKAP350KD cells showed an impairment in MTOC translocation towards the activating
118 surface. Therefore, AKAP350 participates in MTOC translocation by regulating
119 processes that are common to the activation of both LFA-1 and CD28 receptors.

120 4. AKAP350 regulates CIP4 localization in NK cells

121 CIP4 is a CDC42 effector protein involved in regulation of membrane curvature and actin
122 remodeling. In activated NK cells, CIP4 localizes at the MTOC and at the IS and regulates
123 MTOC translocation towards the IS (Banerjee et al., 2007). Considering that, in epithelial
124 cells, AKAP350 interacts with CIP4 and regulates its subcellular localization (Larocca et
125 al 2004, Tonucci et al 2015), we evaluated CIP4 localization at the centrosome in control
126 and AKAP350KD YTS cells. Immunofluorescence analysis by confocal microscopy
127 showed that CIP4 localization at the MTOC was significantly decreased in AKAP350KD
128 YTS cells (Figure 4A). In order to validate those results, subcellular fractions enriched in
129 centrosomes were prepared by differential centrifugation on a Ficoll cushion, and CIP4
130 levels at those fractions were analyzed by western blot. Estimates considering total
131 protein recovery and CIP4 band density at total cell lysates and at centrosomal fractions
132 indicated that 3.0 % of total CIP4 localized at the centrosome in control cells, whereas
133 CIP4 yield at centrosomal fraction was reduced to 1.5 % in AKAP350KD cells (Figure
134 4B), thus ratifying that AKAP350 participates in CIP4 recruitment to the centrosome in
135 YTS cells. In order to analyze the relevance of AKAP350 in CIP4 localization during the

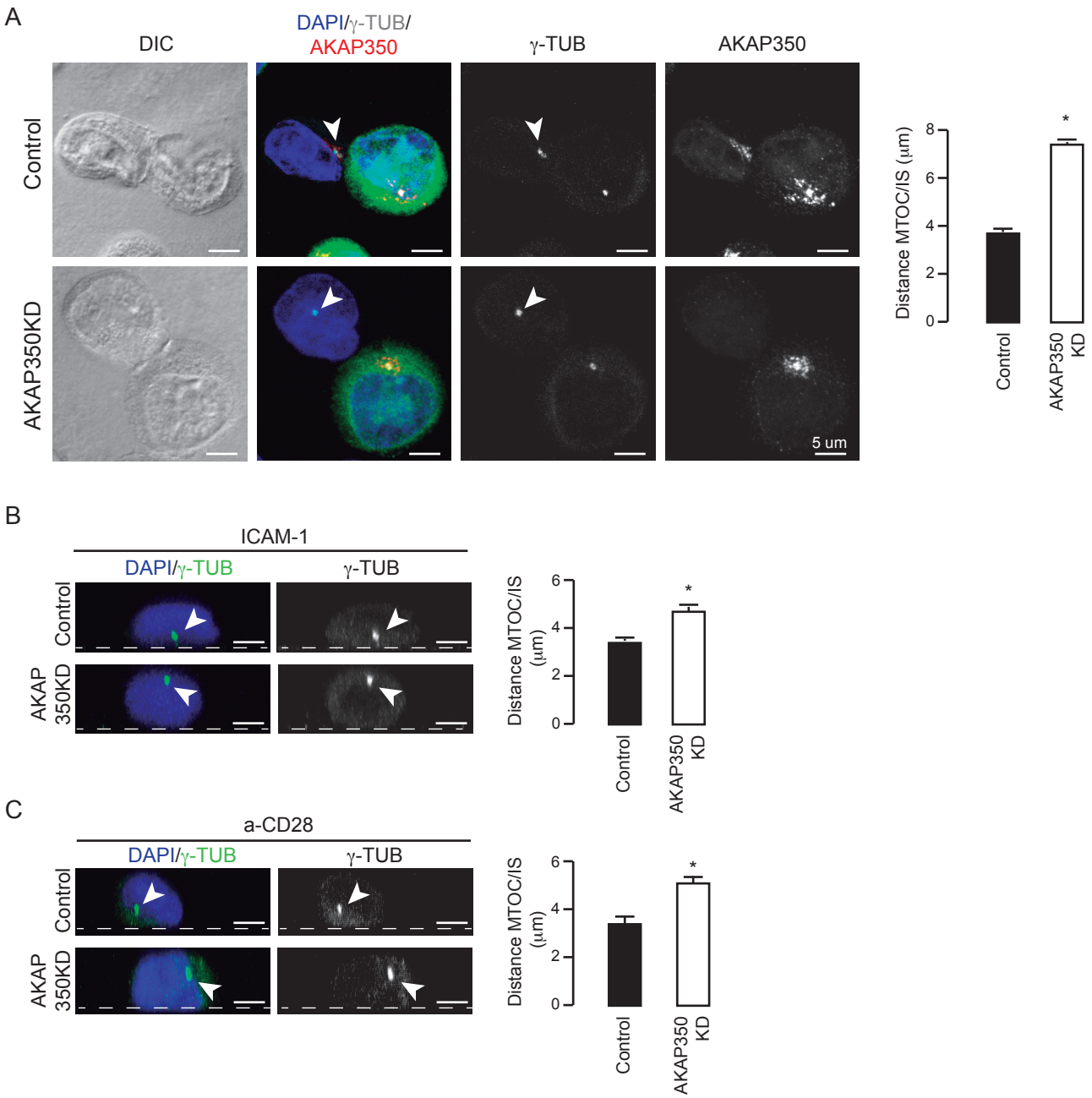

Figure 3. AKAP350 is required for centrosome polarization during YTS cells activation. A) Control and AKAP350KD YTS cells were incubated with CFSE labeled KT86 cells at a 2:1 ratio. Cell conjugates were fixed, stained and analyzed by confocal microscopy. Merge images show staining for AKAP350 (red), γ-tubulin (cyan) and DAPI (blue), and CFSE labeled target cells (green). White arrows indicate the position of γ-tubulin-labeled centrosomes in YTS cells. Bars represent the mean distance from the centrosome to the IS, representative of five independent experiments. B,C) Control and AKAP350KD YTS cells were activated using coverslips coated with the LFA-1 activating ligand ICAM-1 (B) or an activating anti-CD28 antibody (C). Activated cells were fixed, stained and analyzed by confocal microscopy. Merge images show γ-tubulin (green) and DAPI (blue) staining. White arrow indicates the position of γ-tubulin-defined centrosomes. White dashed lines denote the cell surface in contact with the coverslip. Bars represent the mean distance from the centrosomes to the cell-coverslip contact surface, representative of three independent experiments. At least 30 conjugates (A) or cells (B,C) were analyzed for each experiment. Error bars represent SEM. Scale bars, 5 μm. *$p<0.05$.

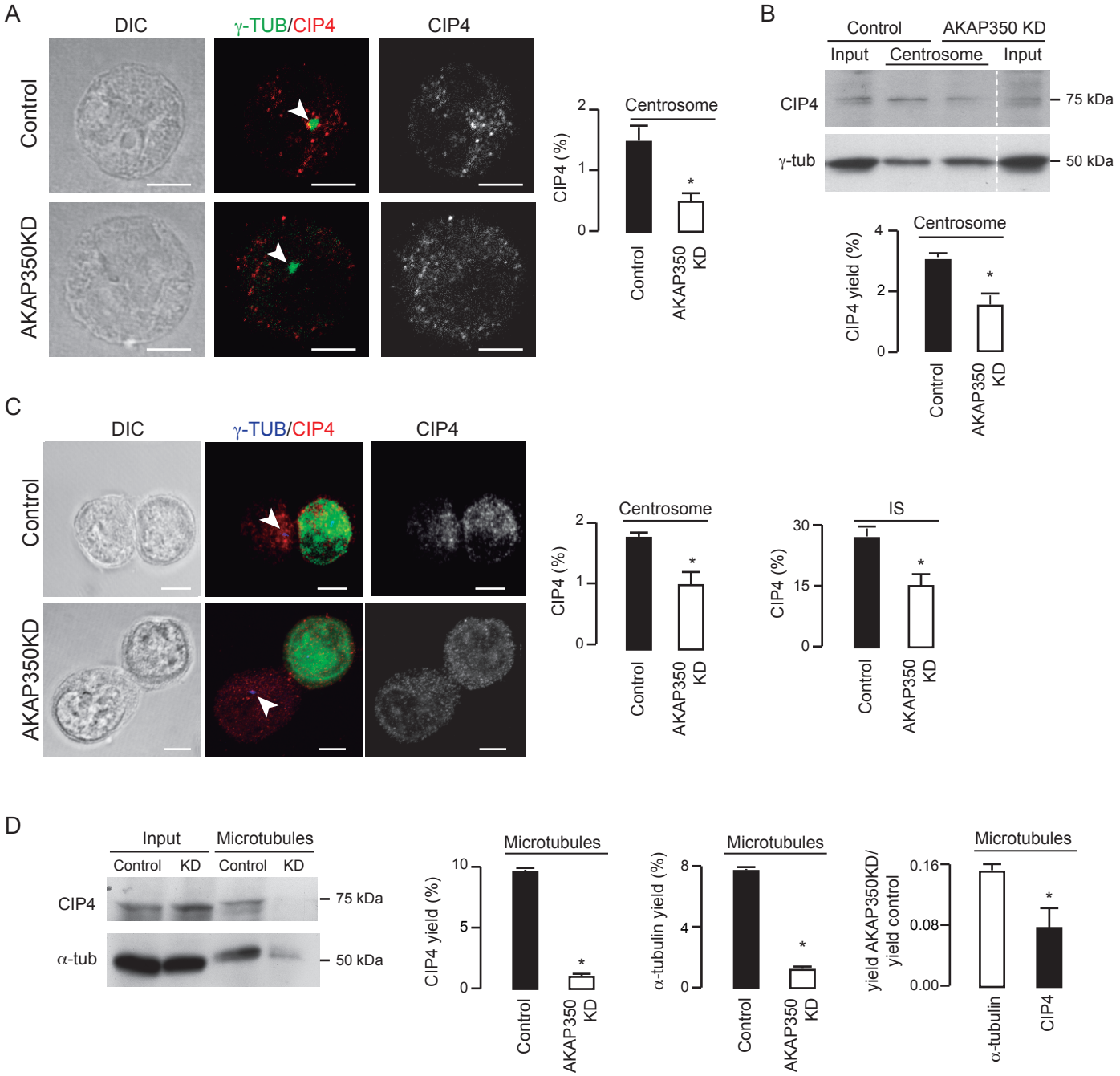

Figure 4. Reduction of AKAP350 expression levels alters CIP4 localization in YTS cells. A) Merge images show staining for CIP4 (red) and γ-tubulin (green) in control and AKAP350KD YTS cells. White arrows mark γ-tubulin defined centrosomes. Bars represent the mean fraction of CIP4 associated fluorescence located at the centrosome, expressed as percentage of total cell fluorescence in the CIP4 channel, representative of three independent experiments. At least 30 conjugates were analyzed for each experiment. Error bars represent SEM. B) Centrosomes enriched subcellular fractions were prepared by differential centrifugation of control or AKAP350KD cell lysates (see Materials and Methods). Total cells lysates and centrosomal fractions were analyzed for CIP4 expression by western blot. Bars represent the mean fraction of CIP4 recovered at centrosome-fractions, expressed as percentage of total CIP4 recovery of three independent experiments. C) CIP4 localization during establishment of the IS was analyzed in control and AKAP350KD YTS:KT86 conjugates (2:1 ratio). Merge images show conjugates staining for CIP4 (red) and γ-tubulin (blue). White arrows indicate the position of γ-tubulin-defined centrosomes. Bars represent the mean fraction of CIP4 fluorescence located at the centrosome or at the IS, expressed as percentage of total cell fluorescence for the CIP4 channel, representative of three independent experiments. At least 30 conjugates were analyzed for each experiment. Error bars represent SEM. D) Control or AKAP350KD cells were incubated in plates coated with the activating anti-CD28 antibody and ICAM-1. Fractions of stabilized microtubules were obtained with non-ionic detergent extraction (see Material and methods). CIP4 and α-tubulin recovery in total cell lysates and microtubule-fractions were analyzed by western blot. Bars represent the mean fraction of CIP4 or α-tubulin recovered at microtubule-fractions, expressed as percentage of total yield in cell lysates, and the mean fraction of CIP4 recovered at the microtubule fraction related to α-tubulin recovery for three independent experiments. Scale bars, 5 μm. *$p < 0.05$

136 development of the lytic IS, CIP4 localization in YTS:KT86 conjugates was analyzed by
137 confocal microscopy. Similarly to our results in resting cells, the analysis of YTS:KT86
138 conjugates showed that CIP4 localization at the centrosome was decreased in
139 AKAP350KD cells (Figure 4C). Furthermore, CIP4 localization at the IS was also
140 impaired in those cells (Figure 4C). By means of its amino-terminal domain CIP4 can
141 interact with the microtubules, therefore, we further analyzed CIP4 in situ interaction with
142 microtubules. Control and AKAP350KD cells were activated with ICAM-1 and extracts
143 of stabilized microtubules and associated proteins were prepared. Western blot analysis
144 of those extracts indicated that a significant fraction of CIP4 was associated with
145 microtubules in control cells and that this fraction was significantly reduced in
146 AKAP350KD cells (Figure 4D). It is noteworthy that α-tubulin recovery in those
147 microtubule extracts was also diminished in AKAP350KD cells. In order to evaluate if
148 this decrease in α-tubulin recovery in microtubule extracts was associated with decreased
149 microtubule stability, we analyzed the relative levels of acetylated α-tubulin in NK cell
150 lysates by western blot. Similarly to what was previously described in motile T cells (Ong
151 et al., 2018), the decrease in AKAP350 expression was associated with a decrease in the
152 levels of acetylated α-tubulin in activated YTS cells, thus indicating decreased
153 microtubule stability in activated AKAP350KD NK cells (Supplementary Figure 2A).
154 CIP4 yield in AKAP350KD microtubule extracts relativized to α-tubulin yield was also
155 reduced (Figure 4D), suggesting that AKAP350 participates in CIP4 recruitment to the
156 microtubule cytoskeleton, independently of its role in the regulation of microtubule
157 stability.

158 5. The decrease in AKAP350 expression impairs actin remodeling in activated NK cells

159 We further analyzed if the decrease in AKAP350 expression had an impact on actin
160 remodeling during NK cell activation. Analysis of YTS:KT86 conjugates by confocal

161 microscopy indicated decreased actin accumulation at the IS in AKAP350KD cells
162 (Figure 5A). Analysis of YTS:KT86 conjugates morphology indicated that the surface of
163 interaction between both cells was also diminished in AKAP350KD cells, which was
164 verified by a reduction in the IS area to 50% of control levels ($p<0.01$). The decrease in
165 the area of effector:target cell interaction is usually associated with decreased integrin-
166 clustering. Consistently, LFA-1 reorganization at the IS was impaired in AKAP350KD
167 cells (Figure 5A). Similarly, inhibition of actin and LFA-1 reorganization was also
168 observed in AKAP350KD cells when they were specifically activated with ICAM-1
169 (Figure 5B) or with the activating anti-CD28 antibody (Figure 5C). The analysis of actin
170 distribution within the IS indicate that control YTS cells showed the characteristic actin
171 pattern of a compact ring in the periphery with less dense actin organization at the center
172 of the IS, whereas AKAP350KD cells showed a more homogeneous actin organization
173 (Figure 5D). LFA-1 clustering at the periphery of the IS was also impaired in
174 AKAP350KD cells (Figure 5D). Those results indicate that AKAP350 participate in
175 regulatory events that enable actin remodeling and LFA-1 clustering at the site of NK-
176 target cell interaction.

177 6. Microtubule cytoskeleton integrity is necessary for LFA-1 organization at the IS

178 In certain conditions, microtubule targeting drugs inhibits NK cytotoxic response (Fong
179 et al., 2019). Nevertheless, microtubule participation in the maturation of NK lytic IS has
180 not been thoroughly evaluated. We analyzed actin remodeling and LFA-1 clustering at
181 the IS in conditions where microtubule integrity was compromised, in the presence of
182 microtubule-targeting drugs at levels that inhibit NK cytotoxicity. We found that neither
183 cold-induced microtubule depolymerization in the presence of Nocodazole nor
184 suppression of microtubule dynamic instability with Taxol have a significant effect on

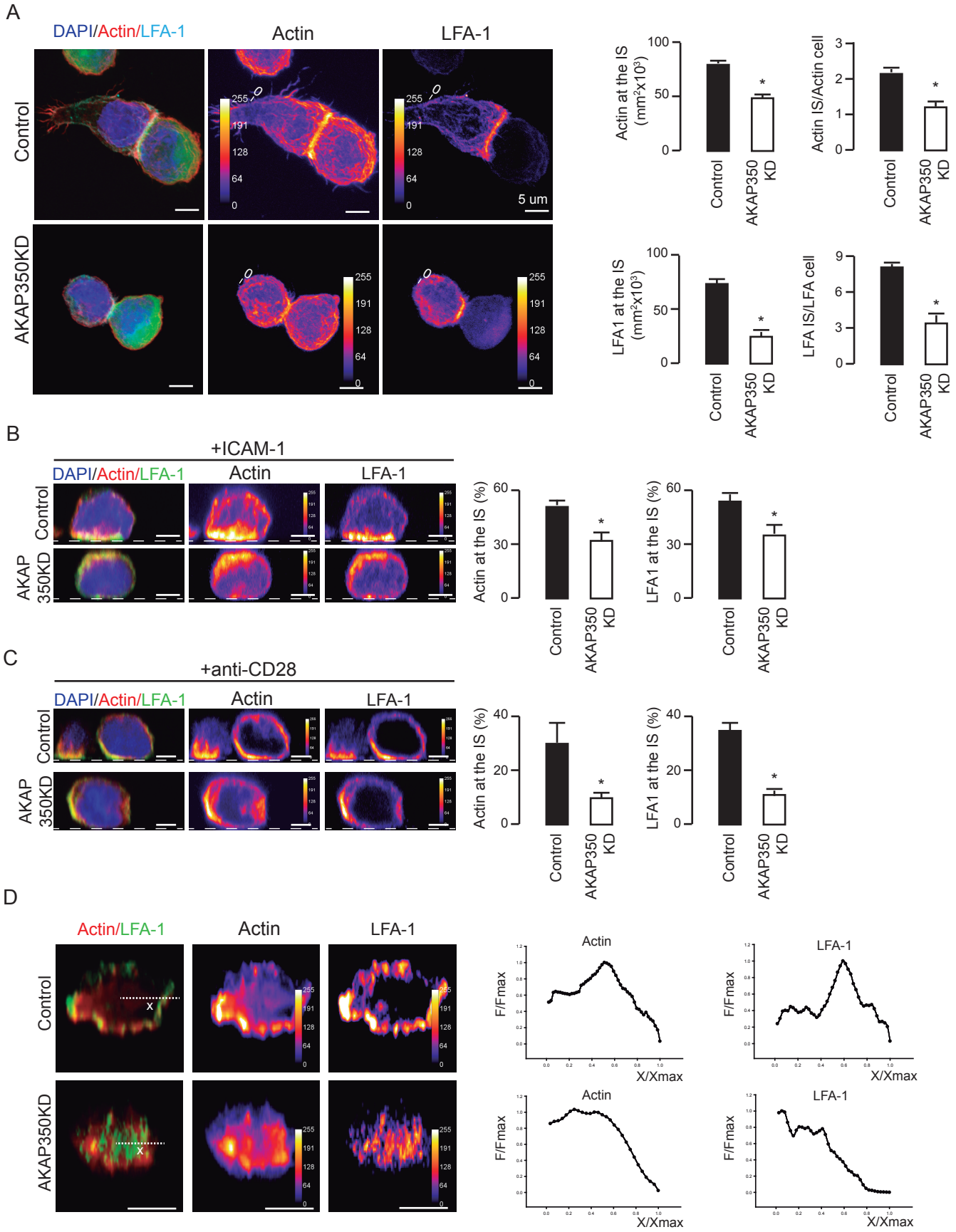

Figure 5. Reduction of AKAP350 expression levels results in defective actin and LFA-1 organization at the IS. A) Control and AKAP350KD YTS cells were incubated with CFSE labeled KT86 cells at a 2:1 ratio. Merge images show YTS:KT86 conjugates staining for actin (red), LFA-1 (cyan) and DAPI (blue). Individual actin and LFA-1 channels are shown in pseudocolor. Bars represent the mean fraction of actin or LFA-1 fluorescence located at the IS, expressed as percentage of total cell fluorescence for each channel, for three independent experiments. At least 30 conjugates were analyzed for each experiment. Error bars represent SEM. B, C) Control and AKAP350KD YTS cells were activated using coverslips coated with ICAM-1 (B) or with the activating anti-CD28 antibody (C).

Merge images show actin (red), LFA-1 (green) and DAPI (blue) staining. Individual actin and LFA-1channels are shown in pseudocolor. White dashed lines indicate the cell surface in contact with the coverslip. Bars represent the mean fraction of actin or LFA-1 fluorescence located at the cell surface in contact with the ICAM-1 (B) or anti-CD28 (C) coated coverslip, expressed as percentage of total cell fluorescence for each channel representative of three independent experiments. At least 30 conjugates were analyzed for each experiment. Error bars represent SEM. D) Control and AKAP350KD YTS cells were incubated with CFSE labeled KT86 cells. Images show the X-Z projection of the IS region corresponding to control and AKAP50KD YTS cells. Merge images show LFA-1 (green) and actin (red) staining. Individual LFA-1 and actin channels are shown in pseudocolor. Dashed lines denote the radius of the IS where LFA-1 and actin intensity of fluorescence were quantified. Charts represent the profile of intensity of fluorescence quantified for each channel, representative of at least ten IS analyzed in three independent experiments. Scale bars, 5 μm. *$p<0.05$.

185 total actin accumulation at the IS (Figure 6). Regarding LFA-1 distribution at the IS, both
186 treatments elicited similar effects, inhibiting LFA-1 accumulation (Figure 6A) and
187 organization (Figure 6B) at the IS.

188 7. AKAP350 participates in microtubule nucleation at the Golgi apparatus in activated
189 NK cells

190 Previous studies demonstrate that AKAP350 can modulate microtubule nucleation at the
191 Golgi apparatus and at the centrosomes in different systems (Takahashi et al, 2002;
192 Rivero et al, 2009; Ori-McKenney et al, 2012; Maia et al, 2013; Tonucci et al, 2018). To
193 our knowledge, microtubule nucleation at the Golgi apparatus in NK cells has not been
194 analyzed so far. Therefore, we analyzed microtubule nucleation at the centrosome and at
195 the Golgi apparatus in activated YTS cells, using ice recovery assays as previously
196 described (Grimaldi et al, 2013). In conditions of YTS cell activation with ICAM-1 and
197 anti-CD28 receptor antibody, control cells showed Golgi and centrosome nucleation of
198 microtubules (Figure 7, first row). AKAP350KD cells, in contrast, showed almost
199 exclusive centrosome nucleation of microtubules (Figure 7, second row). Quantitative
200 analysis of newly nucleated microtubules indicated a significant reduction in Golgi
201 associated microtubules in AKAP350KD cells (Figure 7, upper bars), whereas no
202 differences were observed for centrosome-associated microtubules (Figure 7, lower bars).
203 Similar results were obtained at 3 min (Figure 7) or 7 min (not shown) of recovery.

204 8. Golgi apparatus integrity is essential for the IS maturation in NK cells

205 As delineated above, during YTS cell activation AKAP350 translocates to the Golgi
206 apparatus (Figure 1) where it is essential for microtubule nucleation (Figure 7). In order
207 to analyze if AKAP350 participation in NK IS maturation could be associated with its
208 function at the Golgi apparatus, we analyzed the IS development in NK cells subjected to

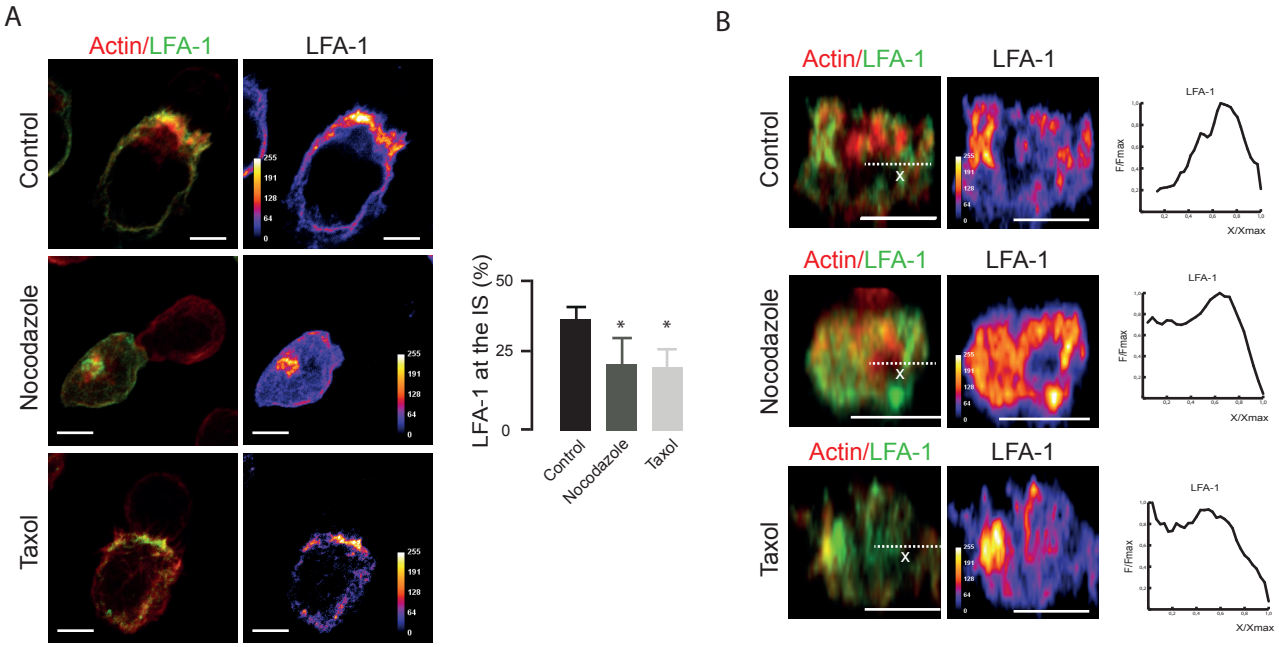

Figure 6. Microtubule dynamics is required for LFA-1 organization at the IS. Control YTS cells or YTS cells treated with nocodazole or taxol (see Materials and methods) were mixed with KT86 cells at a 2:1 ratio. Images show x,y planes (A) or x,z projections (B) of the IS region corresponding to control and nocodazole or taxol treated YTS cells. Merge images show cell conjugates staining for actin (red) and LFA-1 (green). LFA-1 channel is also shown in pseudocolor. A) Bars represent the mean fraction of LFA-1 fluorescence located at the IS, expressed as percentage of total cell fluorescence, representative of three independent experiments. At least 30 conjugates were analyzed for each experiment. B) Dashed lines denote the radius of the IS where LFA-1 intensity of fluorescence was quantified. Charts represent the profile of intensity of fluorescence quantified for the LFA-1 channel, representative of at least ten IS analyzed in three independent experiments. Scale bars, 5 µm. Error bars represent SEM. *$p<0.05$.

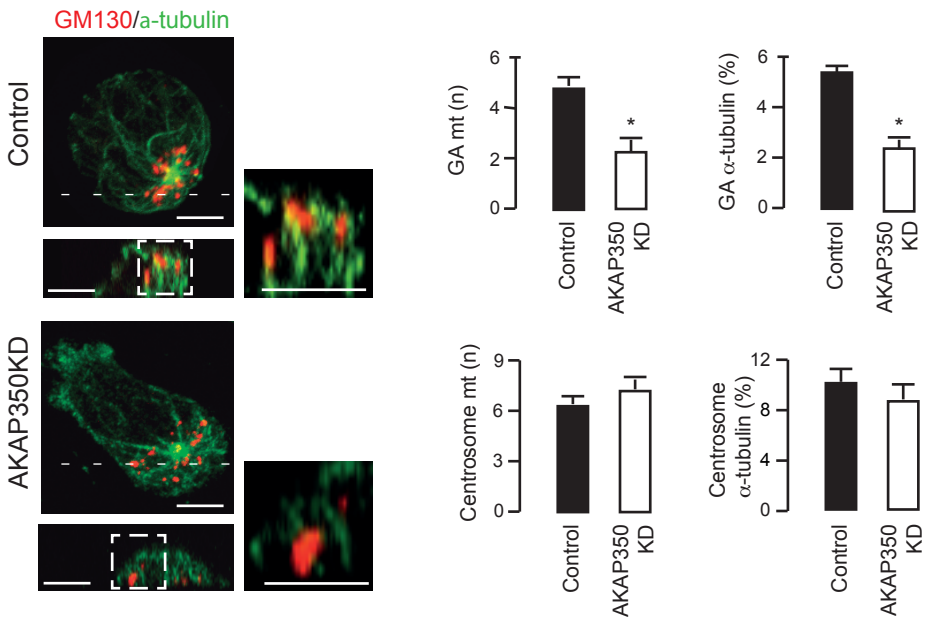

Figure 7. AKAP350 is essential for microtubule nucleation at the Golgi apparatus (GA) in activated YTS cells. Control or AKAP350KD YTS cells were activated using ICAM-1 and anti-CD28 antibody for 30 minutes and then subjected to ice recovery assays. Merge images show staining for GM130, as Golgi marker, in red and for α-tubulin in green. Bar charts represent the mean number of microtubules derived from Golgi apparatus or from the centrosome and the mean fraction of α-tubulin fluorescence associated to each organelle, expressed as percentage of total cell fluorescence for the α-tubulin channel, representative of three independent experiments. At least 10 cells were analyzed for each experiment. Error bars represent SEM. Scale bars, 5 μm. *p<0.05

209 Brefeldin A (BFA) treatment. BFA inhibits the activation of ADP-ribosylation factors,
210 leading to the collapse of the Golgi and its redistribution into the ER (Chardin and
211 McCormick, 1999). Previous studies showed that BFA treatment induced relocalization
212 of AKAP450 from the Golgi apparatus to ER exit sites and decreased MT nucleation at
213 the Golgi apparatus (Rivero et al. 2009). Analysis of LFA-1 distribution at the IS showed
214 that BFA-treatment inhibited LFA-1 organization at the IS (Figure 8A,B). Interestingly,
215 actin organization was preserved in BFA treated cells (data not shown). To specifically
216 examine the relevance of AKAP350 localization at the Golgi in the maturation of NK
217 lytic IS, we prepared YTS cells with stable expression of AKAP350(1-1229)
218 (AKAP350GBD) domain, which acts as a dominant negative construct that displaces the
219 protein from the Golgi apparatus, inhibiting microtubule nucleation at this organelle
220 (Hurtado et al 2011). The analysis of AKAP350 colocalization with GM130 confirmed
221 that AKAP350 localization at the Golgi apparatus was significantly decreased in
222 AKAP350GBD cells (Figure 8C). Relative levels of acetylated α-tubulin were decreased
223 in AKAP350GBD cells (Supplementary figure 2B), suggesting that the decreased α-
224 tubulin acetylation observed in AKAP350KD cells was associated with the decreased
225 expression of AKAP350 at the Golgi apparatus. Similarly to what was observed in BFA
226 treated cells, LFA-1 reorganization was compromised in AKAP350GBD cells (Figure
227 8D,E), whereas actin organization at the IS was preserved. Overall, this set of data
228 showed, for the first time, that the Golgi apparatus is directly involved in LFA-1
229 organization at the IS in NK cells and, considering the evidence presented in Figures 6
230 and 7, gave strong evidence supporting a role for Golgi derived microtubules in this
231 effect.

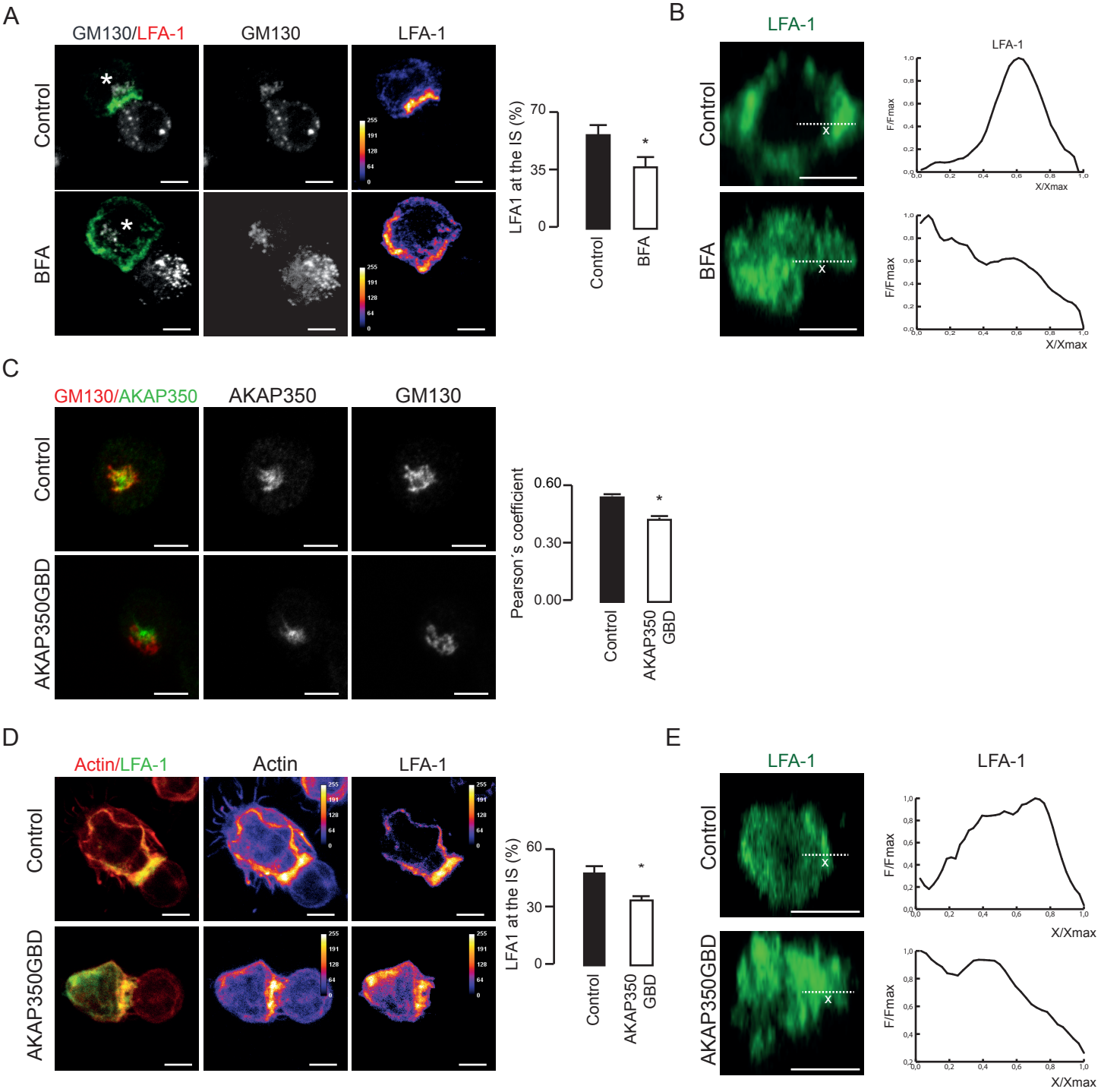

Figure 8. AKAP350 localization at the Golgi apparatus is required for IS maturation. A, B) YTS cells were treated with brefeldin A (BFA) (see Material and methods). A) Control and BFA treated YTS cells were incubated with KT86 cells. Merge images show staining for LFA-1 (green) and GM130 (gray). LFA-1 channel is also shown in pseudocolor. Bars represent the mean fraction of LFA-1 fluorescence located at the IS, expressed as percentage of total LFA-1 cell fluorescence, representative of three independent experiments. B) Images show the x,z projection of the IS region. Dashed lines denote the radius of the IS where LFA-1 intensity of fluorescence was quantified. Charts represent the profile of intensity of fluorescence, representative of at least 10 IS. C-E) YTS cells with stable expression of AKAP350 Golgi binding domain (AKAP350GBD) cells were prepared as described in Materials and methods. C) Merge images show staining for AKAP350 (green) and GM130 (red). Bars represent the mean Pearson´s correlation coefficient, used to estimate AKAP350/GM130 colocalization, for 10 different cells. D,E) Control and AKAP350GBD YTS cells were incubated with KT86 cells. D) Merge images show YTS:KT86 conjugates staining for actin (red) and LFA-1 (green). Individual actin and LFA-1 channels are shown in pseudocolor. Bars represent the mean fraction of LFA-1 fluorescence located at the IS, expressed as percentage of total cell fluorescence. More than 30 conjugates from 3 different experiments were analyzed. E) Images show the x,z projection of the IS region corresponding to control and AKAP350GBD YTS cells. Dashed lines denote the radius of the IS where LFA-1 intensity of fluorescence was quantified. Charts represent the profile of intensity of fluorescence, representative of at least ten IS. Scale bars, 5 µm. Error bars represent SEM. *p<0.05.

232 **Discussion**

233 NK cytotoxic effector function depends on the extensive remodeling of actin and
234 microtubule cytoskeleton, which has been extensively characterized (reviewed in Lagrue
235 et al, 2013). Nevertheless, the mechanisms coordinating cytoskeleton reorganization are
236 not completely understood. In the present study, we provide evidence that AKAP350
237 acts as a scaffold protein that integrates events that are central for both microtubule and
238 actin organization, therefore regulating the development of NK lytic IS. Furthermore, our
239 results indicate that the Golgi apparatus acts as a MTOC in activated NK cells and reveals
240 a novel role for this organelle in the maturation of the lytic IS.

241 In the present study, we found that normal levels of AKAP350 expression are required
242 for MTOC translocation to the IS during the development of NK lytic response. Previous
243 studies by Banerjee and col (2007) demonstrated that CIP4 localizes to the centrosome
244 and to the IS in activated NK cells and that it has a central role in centrosome translocation
245 to the IS. CIP4 is an F-BAR protein initially identified by its ability to interact with the
246 activated form of CDC42 (Aspenström 1997). In the present work, using biochemical and
247 immunofluorescence microscopy-assays, we found that AKAP350 is essential for CIP4
248 localization at the centrosome both in resting and in activated YTS cells. These results
249 give central cues on how CIP4, a protein essentially associated with phospholipid
250 membranes, interacts with the only non-membranous organelle in NK cells and suggest
251 that, homologously to what was described in migratory cells, AKAP350/CIP4 protein
252 complex could act in concert to regulate centrosome translocation towards the IS. Our
253 data further showed that AKAP350 conditions CIP4 localization at the IS. Besides its F-
254 BAR domains, CIP4 also contains a Src Homology 3 (SH3) domain at the carboxyl
255 terminus that mediates its interaction with the proline-rich domains of WASP (Tian et al,
256 2000). WASP is an activator of the Arp2/3 complex that promotes the formation of

257 branched actin filaments, being positively regulated in this function by CDC42 (Leibfried
258 et al., 2008). In NK cells, WASP colocalizes with actin at the IS, playing a central role in
259 the development of the cytotoxic response (Orange et al., 2002). Interestingly, CDC42
260 activity increases at the IS very early during NK cell activation (Carlin et al, 2011). In
261 this scenario, CIP4 could act as an adaptor that enables WASP activation by CDC42 at
262 NK lytic IS. Moreover, by means of its SH3 domain, CIP4 also interacts with formins
263 Dia and DAAM1 (Tsujita et al., 2006; Aspenström et al., 2006). Formins generate linear
264 actin filaments which, in T cells, constitute the central region of the IS and are essential
265 for integrin-clustering and IS maturation (Murugesan et al., 2016). In NK cells, Dia
266 localizes centrally at the IS and participates in targeting microtubules to this site, where
267 lytic degranulation occurs (Butler and Cooper, 2009). Therefore, CIP4 localization at the
268 IS could be central for the maturation of the F-actin-rich SMAC at the IS and microtubule
269 interaction with this site. In this regard, the decrease in CIP4 expression does not affect
270 total actin accumulation at the IS, indicating that CIP4 does not participate in initial actin
271 nucleation, but it is involved in later events that are central for the maturation of the IS
272 (Banerjee et al., 2007). How AKAP350, which specifically localizes to the Golgi
273 apparatus and the centrosome, conditions CIP4 localization at the IS is not clear. In this
274 regard, there is evidence supporting two putative mechanisms: 1. AKAP350 regulates
275 CIP4 T225 phosphorylation by PKA, which controls its localization in invadopodia and
276 CIP4 interaction with CDC42 (Tonucci et al., 2019); similarly, AKAP350 could integrate
277 regulatory events that condition CIP4 localization at the IS. 2. CIP4 recovery in
278 microtubule extracts was decreased in AKAP350KD cells. As we discuss below,
279 microtubule dynamics is altered in AKAP350KD cells. Therefore, AKAP350 could
280 regulate CIP4 localization at the IS by enabling cellular events that condition CIP4
281 trafficking towards the IS.

282 Microtubules can regulate actin remodeling in dissimilar scenarios where polarized actin
283 organization is required, such as integrin mediated phagocytosis (Lewkowicz et al.,
284 2008), directional cell migration (Waterman-Storer & Salmon, 1999) and epithelial apical
285 pole-differentiation (Mattaloni et al, 2012; Tonucci et al, 2018). Microtubule´s role in
286 actin-organization at the IS was not clear. Microtubule targeting agents have paradoxical
287 effects on NK cells cytotoxicity, what seems to be related to the concentration and the
288 type of microtubule targeting agent evaluated (Katz et al., 1982; Fong et al., 2019). We
289 found that levels of nocodazole that actually inhibits NK cytotoxicity (Katz et al., 1982),
290 impair LFA-1 organization at the IS, but does not elicit any evident effect on actin
291 organization. Orange et al have previously demonstrated that neither cell-surface receptor
292 nor F-actin accumulation at the activating NK IS were disrupted with colchicine (Orange
293 et al., 2003). Colchicine and nocodazole have similar mechanisms of action: both drugs
294 bind to the β tubulin subunit blocking α/β heterodimers polymerization (Florian and
295 Mitchison 2016). Nevertheless, in our study we additionally induced microtubule
296 depolymerization by ice incubation, which leads to a more robust disruption of
297 microtubule integrity. Our results also showed that micromolar levels of the microtubule
298 stabilizing agent Taxol, which impedes microtubule growing and shortening events
299 (Derry et al., 1995) and inhibit NK cytotoxicity (Chuang et al., 19941), did not affect
300 actin accumulation or organization, but inhibited LFA-1 reorganization at the IS. At
301 micromolar levels, taxol inhibits the association of microtubule plus end binding proteins
302 such as EB1 (Morrison et al., 1998) and CLIP170 (Perez et al., 1999). Therefore,
303 microtubule dynamic instability and/or the presence of specific microtubule plus end
304 binding proteins could be required for LFA-1 reorganization at the IS. In this regard, in
305 T cells, the α-tubulin deacetylase HDAC6, translocates to the IS where it regulates α-
306 tubulin deacetylation and LFA-1 organization (Serrador et al., 2004). HDAC6 increases

307 microtubule dynamics instability, which correlates with its interaction with EB1
308 (Zilberman et al., 2009) and with CLIP170 (Li et al., 2014). Therefore, it would be
309 interesting to investigate if HDAC6 and/or specific microtubule plus end binding proteins
310 are involved in LFA-1 reorganization at the lytic IS in NK cells.

311 Our results demonstrate that, upon NK cell interaction with susceptible targets, AKAP350
312 partially translocates from the centrosome to the Golgi apparatus. Therefore, we analyzed
313 if there was a specific role of AKAP350 at the Golgi apparatus. Even though it is well
314 established that the Golgi apparatus translocates to the IS during NK lytic response
315 (Kupfer et al., 1983), to our knowledge, the role of this organelle in the development of
316 NK lytic IS has not been examined so far. We found that AKAP350 delocalization from
317 the Golgi apparatus inhibits LFA-1 reorganization at the IS, underscoring the relevance
318 of AKAP350 location at this organelle for the development of NK lytic IS. Furthermore,
319 interference with the Golgi apparatus function with BFA, inhibited LFA-1 reorganization
320 at the IS as well, which reassures that the Golgi apparatus has regulatory effects in the
321 maturation of the IS. The presence of AKAP350 at the Golgi apparatus has been mainly
322 associated with the role of this organelle in microtubule nucleation (Rivero et al, 2009,
323 Ori-McKenney et al, 2012; Maia et al, 2013, Tonucci et al, 2018). Microtubule nucleation
324 in lymphocytes has been typically attributed to the centrosome, which, in fact, is
325 commonly denoted as MTOC. We found that LFA-1/CD28 activated NK cells nucleate
326 microtubules both at the centrosome and at the Golgi apparatus. In those conditions, the
327 decrease in AKAP350 expression specifically inhibits microtubule nucleation at the
328 Golgi. Those results are in line with studies that showed that the decrease in AKAP350
329 expression inhibits microtubule nucleation at the Golgi, without having a significant
330 impact on centrosomal nucleation of microtubules (Larocca et al, 2006; Rivero et al,
331 2009; Tonucci et al, 2018). Golgi-derived microtubules are particularly stable, which

332 correlates with their enrichment in post-translationally modified tubulin (reviewed in
333 Sanders et al., 2015). In fact, the study that first characterized the Golgi apparatus role as
334 a MTOC showed that Golgi-nucleated microtubules become rapidly acetylated (Chabin-
335 Brion et al., 2001). A recent study in motile T cells showed that AKAP350 participates
336 in microtubule nucleation at the centrosome and at extra-centrosomal nucleation centers
337 (Ong et al., 2018). Although this study did not identify microtubule nucleation at the
338 Golgi, it showed that the decrease in AKAP350 expression led to decreased levels of
339 acetylated α-tubulin. Consistently, we found that either the decrease in AKAP350
340 expression or its delocalization from the Golgi apparatus elicited a decrease in acetylated
341 α-tubulin levels. Altogether, our results demonstrate that the Golgi apparatus participates
342 in cytolytic IS maturation in NK cells, and strongly suggest that Golgi derived
343 microtubules are involved in this effect. How Golgi-derived microtubules can affect NK
344 cytolytic IS maturation deserves further investigation. In this regard, different studies
345 indicate that those non-radial, highly stable tracks support the directionality of Golgi
346 associated polarized trafficking, (reviewed in Sanders and Kaverina, 2015). In connection
347 with that point, studies performed in T cells show that the Golgi apparatus regulates the
348 two way vesicle trafficking to the IS of signaling proteins that are essential for IS
349 maturation (Carpier et al., 2018). Our future studies will address how this particular set
350 of microtubules modulate Golgi derived trafficking and the relevance of this trafficking
351 for the maturation of the lytic IS in NK cells.

352 **Materials and methods**

353 NK and target cell lines

354 The immortalized NK YTS cells [Drexler, and Matsuo. 2000] and KT86 cells, derived
355 from the MHC class I-negative K562 erythroleukemia cell line stably expressing CD86

356 [Parry et al, 2003], used as susceptible target cells, were obtained from Dr. Jordan Orange
357 lab (Texas Children's Hospital, Houston, TX, USA). Cells were maintained in RPMI
358 medium 1640 supplemented with 10% FBS, 1% L-glutamine, 1% non-essentials amino
359 acids and 1% streptomycin/ampicillin mixture at 37° C and 5% CO_2 atmosphere.

360 In order to prepare YTS cells with reduced expression of AKAP350 (AKAP350KD), we
361 proceeded as we have described previously [Tonucci et al., 2015]. Constructs were made
362 by annealing and ligating oligonucleotides targeting two specific AKAP350 sequences
363 (shRNA1, 5′-CCCAGCTCACTGCTAATTT-3′; shRNA4, 5′-
364 GCAAGAACTAGAACGAGAA-3′) or a scrambled control into the AgeI and EcoRI
365 cloning sites of pLKO.1-puro vector (details at http://www.addgene.org). These
366 constructs were sequenced and used to co-transfect human embryonic kidney 293 FT cells
367 with Virapower lentiviral packaging mix (Invitrogen, Carlsbad, CA). The next day,
368 transfection complexes were removed, and cells were allowed to produce virus for 24 h.
369 Media containing viruses were collected and used to directly transduce YTS cells
370 overnight. The cells were then allowed to recover for 24 h and subjected to puromycin
371 selection (2 μg/ml) for 2 weeks. Silencing was confirmed by western blotting and
372 immunofluorescence analyses.
373 In order to delocalize AKAP350 from the Golgi apparatus, the nucleotide sequence
374 codifying for AKAP350(1-1229) (AKAP350GBD) was cloned into pInducer20 vector
375 (details at http://www.addgene.org). The lentiviral particles were constructed as described
376 above. Transduced YTS cells were subjected to G418 selection (1 μg/ml) for two weeks.
377 AKAP350GBD expression was induced with Doxycycline (2 μg/ml) 24 h before the
378 experiments.
379 CFSE-based Cytotoxic assay

380 In order to determine the lytic capacity of YTS cells, we proceed as described [Jedema et
381 al. 2004]. KT86 cells were washed with PBS, resuspended at 2 x10^6 cells/mL and labeled
382 with 300 nM CFSE (BD Horizont) for 15 min at 37°C. The reaction was stopped by the
383 addition of an equal volume of fetal bovine serum (FCS), followed by a 2-min incubation
384 at room temperature. CFSE-labeled target cells were washed twice and resuspended in
385 RPMI complete medium. The cell concentration was adjusted to 5 x 10^5 cells/mL, and
386 100 µL/tube were plated in Eppendorf tubes. YTS cells were added at different
387 effector:target ratios. Tubes were incubated in a humidified atmosphere of 5% CO2 and
388 37°C for 3 hours. For dead cells staining, propidium iodide (1 µg/mL) was added, and
389 samples were mixed properly and directly analyzed by flow cytometry using a BD
390 FACSAria II flow cytometer. 10000 events were acquired for each sample. Double
391 positive events for CFSE and PI were considered dead target cells. The percentage of
392 specific lysis was calculated as follows: specific lysis (%) = [(Double positive cells -
393 spontaneous dead cells) / CFSE positive cells] x 100.
394 FACS-based conjugation assay
395 YTS cells were washed with PBS, resuspended to 1 x 10^6 cells/ml and labeled with 1.5
396 mM Cell TrackerTM Deep Red (Invitrogen) for 20 min at 37° C. The reaction was
397 stopped by the addition of an equal volume of fetal bovine serum, followed by a 5 min
398 incubation at room temperature. After two washes with PBS, the YTS-labeled cells were
399 resuspended in RPMI complete medium. Target cells were labeled with 300 nM CFSE
400 (BD Horizon) as described above. Cells were combined at an effector to target ratio of
401 2:1 or 10:1 and incubated at 37º C for different periods, as indicated. The samples were
402 gently vortexed for 3 s and immediately fixed with 2% paraformaldehyde (PFA). Samples
403 were run in triplicates and 50000 events were counted for each replicate. The frequency
404 of double positive events was determined within the CFSE positive population using

405 FlowJo software. The following gating strategy was used: First, cells were gated to
406 exclude debris. Compensation adjustments were made on this population using single-
407 positive cells stained for either Cell TrackerTM Deep Red or CFSE. Gates were set to
408 differentiate between the double positives from the single positives and double negatives.
409 Immunofluorescence
410 KT86 were labeled with 300 nM CFSE (BD Horizon) as described above. Conjugates
411 between YTS cells and KT86 at a 2:1 ratio were established in suspension for 15 min at
412 37 ° C and adhered to poly-lysine-coated glass slides (Polyprep; Sigma-Aldrich) for
413 additional 15 min. In experiments evaluating NK cell activation by means of specific
414 activating receptors, poly– l -lysine – coated glass slides were coated with anti-CD28, or
415 ICAM-1 by overnight incubation in PBS. Slides were washed, and NK cells were
416 incubated on the slide for 30 min at 37 ° C. Non adherent cells were washed and cells
417 adhering to the slide were fixed with 4% PFA at room temperature or methanol at -20°
418 C. Fixed cells were permeabilized and blocked with 0.3%Triton X-100/1% bovine serum
419 albuminin/PBS, pH 7.4, for 10 min. Then, they were incubated for 2 h with mouse
420 monoclonal antibody anti CIP4 (BD transduction-612556), anti-LFA-1 (Biolegend
421 301202) or anti AKAP350 (Schmidt et al, 2001) and rabbit monoclonal antibody anti γ-
422 tubulin (Sigma-T5192) . The coverslips were washed, incubated for 1 h with the
423 secondary antibodies conjugated to Alexa 488, Alexa 560 or Alexa 633 or with
424 phalloidin-Alexa 568 (Molecular probes-A34055, 1:200) for actin staining and with 4′,6-
425 diamidino-2-phenylindole (DAPI) and mounted with ProLong (Invitrogen). Fluorescence
426 was detected using LSM880 confocal with an ObserverZ1 inverted microscope. Serial
427 optical 0.2 μm thick sections were collected in the z-axis. Z-stacks were built, and
428 projections were obtained using ImageJ tools. In preparing the figures, adjustment in

429 brightness and contrast were equally applied to the entire images using Adobe Photoshop
430 software to improve visualization of fluorescence.

431 Image analysis

432 Centrosome polarization during IS formation. YTS:KT86 conjugates were stained with
433 anti γ-tubulin and DAPI, for centrosome and nucleus identification. The IS was defined
434 as the cell to cell contact region identified in the images obtained by differential
435 interference microscopy (DIC). The cell perimeter of the YTS cell forming the IS was
436 drawn using the same images. The centrosome region was delimited by setting a threshold
437 on the γ-tubulin channel to define a mask, which was used to automatically outline the
438 centrosomal pixels. The IS, centrosome, and cell centroid were determined using the
439 appropriate ImageJ tool and the distances from the cell or the centrosome centroid to the
440 IS centroid were calculated. Alternatively, for analysis of centrosome translocation during
441 specific LFA-1 or CD28 activation, the surface of YTS interaction with the ICAM-1 or
442 anti-CD28 coated slides was considered as the IS site, and the distance was measured at
443 the *(y,z)* plane where the centrosome was best visualized. At least 30 cells from three
444 independent experiments were analyzed for each condition.

445 For protein accumulation at the IS, YTS cells conjugated with KT86 cells were analyzed.
446 We used DIC images for IS and cell selections, as described above. We measured
447 fluorescence intensity at YTS IS and at the YTS cell (T). The percentage of protein
448 accumulation was calculated as the ratio IS*100/T.

449 Centrosomal localization of CIP4 or AKAP350 was determined in images obtained by
450 confocal microscopy by setting a threshold on the γ-tubulin channel as described above,
451 and a threshold on CIP4 or AKAP350 channels to define a mask to automatically outline
452 total voxels for each protein staining. Average and total intensity of fluorescence in CIP4

453 or AKAP350 channels was measured in each region of interest, and the percentage of
454 centrosomal levels for each protein calculated.
455 Golgi levels of AKAP350 were determined in images obtained by confocal microscopy
456 by setting a threshold on GM130 channel to define a mask, which was used to
457 automatically outline the Golgi voxels. Total intensity of fluorescence in the AKAP350
458 channel was measured in each region of interest. In addition, total AKAP350 levels were
459 determined in a region delimited by a mask defined using the AKAP350 channel, and the
460 percentage of AKAP350 fluorescence at the Golgi apparatus calculated. AKAP350
461 colocalization with GM130 in AKAP350GBD cells was determined by estimating the
462 Pearson´s coefficient using the Image J colocalization tools.
463 Immunoblotting
464 Cells were harvested at 400 *g* for 5 min at room temperature and washed with cold PBS.
465 Pelleted cells were lysed in ice-cold lysis buffer (50 mM Tris-HCl [pH 7.5], 100 mM
466 NaCl, 15 mM EDTA and 1% Triton X-100, supplemented with protease inhibitors) and
467 subjected to two freeze–thaw cycles. Lysates were centrifuged at 1000 *g* for 5 min at 4°
468 C, and the clear supernatants were conserved. Total protein concentration was measured
469 according to Lowry *et al*. (1951). Samples were heated for 10 min at 90 °C in sample
470 buffer (20 mM Tris-HCl, pH 8.5, 1% SDS, 400 µM DTT, 10% glycerol). Samples
471 containing equal amounts of proteins were subjected to SDS polyacrylamide gel
472 electrophoresis (6–10% gradient to assess AKAP350 levels or 10% otherwise). The
473 proteins in the 6% gel were transferred to nitrocellulose membranes (Amersham
474 Pharmacia Biotech), whereas the 10% gel proteins were transferred to polyvinyl
475 difluoride membranes (Perkin Elmer Life Sciences). Blots were blocked with 5% nonfat
476 dry milk in PBS, 0.3% Tween-20 (PBS-Tween). Nitrocellulose blots were then probed
477 with the monoclonal mouse anti-AKAP350 antibody (1:500), and polyvinyl difluoride

478 membranes were probed with mouse monoclonal antibodies anti-α-tubulin (Sigma-
479 T9026, 1:5000), anti-γ-tubulin (Sigma-T6557, 1:2000) or anti-CIP4 (BD transduction-
480 612556, 1:500). The blots were washed and incubated with the horseradish peroxidase-
481 conjugated corresponding secondary antibodies, and bands were detected by enhanced
482 chemiluminescence (Pierce, Thermo Scientific). Autoradiographs were obtained by
483 exposing the blots to Kodak XAR film. The bands were quantitated by densitometry using
484 the NIH Image J program.

485 Preparation of centrosome and microtubule enriched subcellular fractions.

486 Centrosome-enriched fractions were prepared by centrifugation on a Fycoll cushion,
487 using a method based on Blomberg-Wirschell and Doxsey [1998]. Briefly, cells were
488 treated with Nocodazole (1.65 μM) and Cytochalasin (390 ηM) for 30 min, and washed
489 with PBS. Cells were resuspended and gently sonicated in a lysis buffer containing 1Mm
490 TRIS-HCl [pH 8], 0.5% β-Mercaptoethanol, 0.5% Triton X-100 and protease inhibitors.
491 Components were added to cell lysates to achieve a final concentration of 10 mM PIPES,
492 1 mM EDTA. In order to eliminate unbroken cells and nuclear fractions, cell extracts
493 were centrifuged at 1,500 *g* for 15 min. The supernatant was filtered through a nylon mesh
494 and loaded on the top of a 20% (w/v) Ficoll cushion in buffer 10 mM PIPES/1 mM EDTA
495 with 0.1% Triton X-100 and tubes were spun at 25,000 g in a swinging bucket rotor.
496 Centrosomes were taken from the top of the Ficoll cushion using a Pasteur pipet, and
497 CIP4 levels at this fraction were analysed by western blot.

498 Cellular extracts enriched in stable microtubules were prepared based on a non-ionic
499 detergent extraction protocol described by Brown et al (1992). A total of $4x10^6$ YTS cells
500 were harvested and added on plastic wells coated with ICAM-1 and CD28 for 30 minutes
501 at 37°C. Cells were rinsed once with PBS and once with PHEM (60 mM Pipes, 25 mM
502 Hepes, 10 mM EGTA, 2 mM MgC12, pH 6.9) and then extracted for 5 min in PHEM

503 containing 0.1% Tritón X-100, 10 µM taxol and a mixture of protease inhibitors. Then,
504 the cells were washed with PHEM without Tritón and scrapped with a 100 µL of sample
505 buffer. The protein-contained sample buffer was collected into eppendorf tubes and
506 incubated for 10 minutes at 90°C . The proteins associated with microtubules were
507 analyzed by western blot.

508 YTS cells treatments

509 In order to assess the role of microtubules in the IS formation, YTS cells were harvested
510 and 2.10^6 cells were treated for 1 hour with nocodazole (17 µM) on ice or for 1 hour or
511 with taxol (10 µM) at room temperature and then allowed to form conjugates with KT86
512 cells at a 2:1 ratio for 15 min at 37° C. In order to evaluate the role of the Golgi apparatus
513 in IS formation, YTS cells were treated with Brefeldin A (5 µg/ml) for 30 min at 37 °C.
514 After Brefeldin A treatment, YTS cells were allowed to form conjugates with KT86 cells
515 at a 2:1 ratio for 15 min at 37 °C. YTS cells without treatment were used as control for
516 each experiment. Conjugates were analyzed by confocal microscopy as described above.

517 Ice recovery assay

518 A total of $2x10^5$ YTS cells were placed on poly-l-lysine-coated coverslips coated with
519 ICAM-1 and CD28 and incubated for 30 minutes at 37°C. Then, coverslips were
520 incubated on ice 50 min and allowed to recover at room temperature. For analysis of
521 Golgi and centrosome nucleation of microtubules, cells were recovered for 3 or 7 minutes
522 and immediately treated 45 s with extraction buffer (60 mM PIPES, 25 mM HEPES, 10
523 mM EGTA, 2 mM MgCl2, 0.1% Tritón X-100, pH 6.9, supplement with 0.25 nM
524 nocodazole and 0.25 nM taxol). Cells were then fixed with methanol and stained with
525 antibody anti GM130 (Abcam-EP892Y) and antibody anti α-tubulin (Sigma-T9026).

526 **Acknowledgments**

527 We thank Dr. Andrés Zucchetti for his critical discussion of the manuscript. This work
528 was supported by Grants PUE 0089 from CONICET and PICT2015-2755 and PICT2016-
529 4758 from ANPCyT. The funders had no role in study design, data collection and
530 analysis, decision to publish, or paper preparation.

531 **Competing interests**

532 There are not competing interests to declare.

533 **References**

534 Aspenström PA. Cdc42 target protein with homology to the non-kinase domain of FER
535 has a potential role in regulating the actin cytoskeleton. *Curr Biol*. 1997; 7: 479-87. DOI:
536 https://doi.org/10.1016/S0960-9822(06)00219-3

537 Aspenström P, Richnau N, Johansson AS. The diaphanous-related formin DAAM1
538 collaborates with the Rho GTPases RhoA and Cdc42, CIP4 and Src in regulating cell
539 morphogenesis and actin dynamics. Exp. Cell Res. 2006; 312:2180-2194. DOI:
540 https://doi.org/10.1016/j.yexcr.2006.03.013

541 Banerjee PP, Pandey R, Zheng R, Suhoski MM, Monaco-Shawver L, Orange JS. Cdc42-
542 interacting protein-4 functionally links actin and microtubule networks at the cytolytic
543 NK cell immunological synapse. J Exp Med. 2007; 204:2305-20. DOI:
544 10.1084/jem.20061893

545 Blomberg-Wirschell, M. & Doxsey, S. J. Rapid isolation of centrosomes. *Methods*
546 *Enzymol.* **298**, 228–38 (1998). DOI: 10.1016/s0076-6879(98)98022-3

547 Brown ACN, Oddos S, Dobbie IM, Alakoskela J-M, Parton RM, et al. (2011)
548 Remodelling of Cortical Actin Where Lytic Granules Dock at Natural Killer Cell Immune

549 Synapses Revealed by Super-Resolution Microscopy. PLoS Biol 9(9): e1001152. DOI:
550 10.1371/journal.pbio.1001152

551 Brown A, Slaughter T, Black MM. Newly Assembled Microtubules Are Concentrated in
552 the Proximal and Distal Regions of Growing Axons. J Cell Biol. 1992; 119: 867-882.
553 DOI: 10.1083/jcb.119.4.867.

554 Butler B, Cooper JA. Distinct roles for the actin nucleators Arp2/3 and hDia1 during NK-
555 mediated cytotoxicity. Curr Biol 2009; 19: 1886–1896. DOI: 10.1016/j.cub.2009.10.029.

556 Carlin LM, Evans R, Milewicz H, Fernandes L, Matthews DR, Perani M, Levitt J,
557 Keppler MD, Monypenny J, Coolen T, Barber PR, Vojnovic B, Suhling K, Fraternali F,
558 Ameer-Beg S, Parker PJ, Thomas NS, Ng T. A targeted siRNA screen identifies
559 regulators of Cdc42 activity at the natural killer cell immunological synapse Sci Signal.
560 2011; 4:ra81. DOI: 10.1126/scisignal.2001729

561 Carpier JM et al. Rab6-dependent retrograde traffic of LAT controls immune synapse
562 formation and T cell activation. J. Exp. Med. (2018) 215, 1245–1265. DOI:
563 10.1084/jem.20162042

564 Chabin-Brion K, Marceiller J, Perez F, Settegrana C, Drechou A, Durand G, Poüs C . The
565 Golgi complex is a microtubule-organizing organelle. Mol Biol Cell. 2001; 12:2047-60.
566 DOI: 10.1091/mbc.12.7.2047

567 Chardin P, McCormick F. Brefeldin A: The Advantage of Being Uncompetitive. Cell.
568 1999; 97:153-155. DOI: 10.1016/s0092-8674(00)80724-2

569 Chen X, Allan DS, Krzewski K, Ge B, Kopcow H, Strominger JL. CD28-stimulated
570 ERK2 phosphorylation is required for polarization of the microtubule organizing center
571 and granules in YTS NK cells. Proc. Natl. Acad. Sci. USA. 2006; 103:10346–10351.
572 DOI: 10.1073/pnas.0604236103

573 Chuang, L.T.; Lotzová, E.; Heath, J.; Cook, K.R.; Munkarah, A.; Morris, M.; Wharton,
574 J.T. Alteration of lymphocyte microtubule assembly, cytotoxicity, and activation by the
575 anticancer drug taxol. Cancer Res. 1994, 54, 1286–1291.

576 Derry WB, Wilson L, Jordan MA. Substoichiometric Binding of Taxol Suppresses
577 Microtubule Dynamics. Biochemistry 1995,34, 2203-2211. DOI: 10.1021/bi00007a014

578 Drexler, H. G., Y. Matsuo. 2000. Malignant hematopoietic cell lines: in vitro models for
579 the study of natural killer cell leukemia-lymphoma. Leukemia 14: 777-782. DOI:
580 10.1038/sj.leu.2401778

581 El Din El Homasany BS, Volkov Y, Takahashi M, Ono Y, Keryer G, Delouvée A, Looby
582 E, Long A, Kelleher D. 2005. The scaffolding protein CG-NAP/AKAP450 is a critical
583 integrating component of the LFA-1-induced signaling complex in migratory T cells. J
584 Immunol. 175:7811-8. DOI: 10.4049/jimmunol.175.12.7811

585 Florian S, Mitchison TJ. Anti-Microtubule Drugs. Methods Mol Biol. 2016;1413:403-21.
586 doi: 10.1007/978-1-4939-3542-0_25. DOI: 10.1007/978-1-4939-3542-0_25

587 Fong A, Durkin A, and Lee H. Int. The Potential of Combining Tubulin-Targeting
588 Anticancer Therapeutics and Immune Therapy. J. Mol. Sci. 2019, 20, 586;
589 doi:10.3390/ijms20030586. DOI: 10.3390/ijms20030586

590 Grimaldi AD, Fomicheva M, Kaverina I. Ice recovery assay for detection of Golgi-
591 derived microtubules. Methods Cell Biol. 2013; 118:401-15. DOI: 10.1016/B978-0-12-
592 417164-0.00024-0

593 Hurtado L, Caballero C, Gavilan MP, Cardenas J, Bornens M, Rios RM. Disconnecting
594 the Golgi ribbon from the centrosome prevents directional cell migration and ciliogenesis.
595 J Cell Biol. 2011 May 30;193(5):917-33. DOI: 10.1083/jcb.201011014

596 Jedema, Inge, et al. New CFSE-based assay to determine susceptibility to lysis by
597 cytotoxic T cells of leukemic precursor cells within a heterogeneous target cell
598 population. *Blood* 103.7 (2004): 2677-2682. DOI: 10.1182/blood-2003-06-2070

599 Katz P, Zaytoun AM and Lee J H Jr. Mechanisms of human cell-mediated cytotoxicity.
600 III. Dependence of natural killing on microtubule and microfilament integrity. J Immunol
601 1982, 129: 2816-2825.

602 Kupfer A, Dennert G, Singer SJ. Polarization of the Golgi apparatus and the
603 microtubule-organizing center within cloned natural killer cells bound to their targets.
604 Proc Natl Acad Sci USA 1983; 80: 7224–7228. DOI: 10.1073/pnas.80.23.7224

605 Kim HS, Takahashi M, Matsuo K, Ono Y. Recruitment of CG-NAP to the Golgi
606 apparatus through interaction with dynein-dynactin complex. Genes Cells. 2007; 12:421-
607 34. DOI: 10.1111/j.1365-2443.2007.01055.x

608 Kolobova E, Roland JT, Lapierre LA, Williams JA, Mason TA, Goldenring JR. The C-
609 terminal region of A-kinase anchor protein 350 (AKAP350A) enables formation of
610 microtubule-nucleation centers and interacts with pericentriolar proteins. J Biol Chem.
611 2017; 292: 20394–20409. doi: 10.1074/jbc.M117.806018. DOI:
612 10.1074/jbc.M117.806018

613 Lagrue K, Carisey A, Oszmiana A, Kennedy PR, Williamson DJ, Cartwright A, Barthen
614 C, Davis DM.. The central role of the cytoskeleton in mechanisms and functions of the
615 NK cell immune synapse. Immunological Reviews 2013. Vol. 256: 203–221. DOI:
616 10.1111/imr.12107

617 Larocca MC, Jin M, Goldenring JR. AKAP350 modulates microtubule dynamics. Eur J
618 Cell Biol. 2006; 85:611-9. DOI: 10.1016/j.ejcb.2005.10.008

619 Larocca MC, Shanks RA, Tian L, Nelson DL, Stewart DM, Goldenring JR. AKAP350
620 interaction with cdc42 interacting protein 4 at the Golgi apparatus. Mol Biol Cell. 2004;
621 15:2771-81. DOI:: 10.1091/mbc.E03-10-0757

622 Leibfried A, Fricke R, Morgan MJ, Bogdan S, Bellaiche Y. Drosophila Cip4 and WASp
623 define a branch of the Cdc42-Par6-aPKC pathway regulating E-cadherin endocytosis.
624 Curr Biol. 2008; 18:1639-48. DOI: 10.1016/j.cub.2008.09.063

625 Li D, Sun X, Zhang L, Yan B, Xie S, Liu R, Liu M, Zhou J. Histone deacetylase 6 and
626 cytoplasmic linker protein 170 function together to regulate the motility of pancreatic
627 cancer cells. Protein Cell. 2014; 5: 214–223. DOI: 10.1007/s13238-013-0010-3

628 Maia A. R., Zhu X., Miller P., Gu G., Maiato H., Kaverina I. (2013). Modulation of Golgi-
629 associated microtubule nucleation throughout the cell cycle. Cytoskeleton 70, 32–43.
630 10.1002/cm.21079. DOI: 10.1002/cm.21079

631 Mace EM, Dongre P, Hsu H-T, Sinha P, James AM, Mann SS, Forbes LR, Watkin LB,
632 Orange JS. Cell biological steps and checkpoints in accessing NK cell cytotoxicity.
633 Immunol Cell Biol. 2014; 92: 245–255. DOI: 10.1038/icb.2013.96

634 Mattaloni SM, Kolobova E, Favre C, Marinelli RA, Goldenring JR, Larocca MC.
635 AKAP350 Is involved in the development of apical "canalicular" structures in hepatic
636 cells HepG2. J Cell Physiol. 2012; 227:160-71. doi: 10.1002/jcp.22713. DOI:
637 10.1002/jcp.22713

638 Morrison MM, Wardleworth BN, Askham JM, Markham AF, Meredith DM. EB1, a
639 Protein Which Interacts With the APC Tumour Suppressor, Is Associated With the
640 Microtubule Cytoskeleton Throughout the Cell Cycle. Oncogene 1998;17(:3471-7. doi:
641 10.1038/sj.onc.1202247. DOI: 10.1038/sj.onc.1202247

642 Murugesan S, Hong J, Yi J, Li D, Beach JR, Shao L, Meinhardt J, Madison G, Wu X,
643 Betzig E, Hammer JA. Formin-generated actomyosin arcs propel T cell receptor
644 microcluster movement at the immune synapse. J Cell Biol. 2016; 215:383-399. DOI:
645 10.1083/jcb.201603080

646 Ong ST, Chalasani MLS, Fazil MHUT, Prasannan P, Kizhakeyil A, Wright GD, Kelleher
647 D, Verma NK. Centrosome- and Golgi-Localized Protein Kinase N-Associated Protein
648 Serves As a Docking Platform for Protein Kinase A Signaling and Microtubule
649 Nucleation in Migrating T-Cells. Front Immunol. 2018; 9:397. DOI:
650 10.3389/fimmu.2018.00397

651 Orange JS, et al. Wiskott-Aldrich syndrome protein is required for NK cell cytotoxicity
652 and colocalizes with actin to NK cell-activating immunologic synapses. Proc Natl Acad
653 Sci USA 2002;99:11351–11356. DOI: 10.1073/pnas.162376099

654 Orange JS, Harris KE, Andzelm MM, Valter MM, Geha RS, Strominger JL. The Mature
655 Activating Natural Killer Cell Immunologic Synapse Is Formed in Distinct Stages. Proc
656 Natl Acad Sci USA. 2003; 100:14151-6. DOI: 10.1073/pnas.1835830100.

657 Ori-McKenney, K. M., Jan, L. Y., & Jan, Y.-N. (2012). Golgi outposts shape dendrite
658 morphology by functioning as sites of acentrosomal microtubule nucleation in neurons.
659 Neuron, 76, 921– 930. DOI: 10.1016/j.neuron.2012.10.008

660 Parry, Richard V., et al. CD28 and inducible costimulatory protein Src homology 2
661 binding domains show distinct regulation of phosphatidylinositol 3-kinase, Bcl-xL, and
662 IL-2 expression in primary human CD4 T lymphocytes. The Journal of immunology,
663 2003, vol. 171, no 1, p. 166-174. DOI: 10.4049/jimmunol.171.1.166

664 Perez, F., G.S. Diamantopoulos, R. Stalder, and T.E. Kreis. 1999. CLIP-170 highlights
665 growing microtubule ends in vivo. Cell. 96:517–527. DOI: 10.1016/s0092-
666 8674(00)80656-x

667 Rak GD, Mace EM, Banerjee PP, Svitkina T, Orange JS. 2011. Natural killer cell lytic
668 granule secretion occurs through a pervasive actin network at the immune synapse. PLoS
669 Biol 9:e1001151. DOI: 10.1371/journal.pbio.1001151.

670 Rivero S, Cardenas J, Bornens M, Rios RM. Microtubule nucleation at the cis-side of the
671 Golgi apparatus requires AKAP450 and GM130. EMBO J. 2009, 281016-28. DOI:
672 10.1038/emboj.2009.47

673 Roberts-Galbraith RH & Gould KL. Setting the F-BAR: functions and regulation of the
674 F-BAR protein family. *Cell Cycle* 2010; 9:4091-4097. DOI: 10.4161/cc.9.20.13587

675 Robles-Valero J, Martín-Cófreces NB, Lamana A, Macdonald S, Volkov Y, Sánchez-
676 Madrid F. (2010) Integrin and CD3/TCR activation are regulated by the scaffold protein
677 AKAP450. Blood. 115:4174-84. DOI: 10.1182/blood-2009-12-256222

678 Sanders AA, Kaverina I. Nucleation and dynamics of Golgi-derived microtubules. Front
679 Neurosci. 2015;9:431. doi: 10.3389/fnins.2015.00431. DOI: 10.3389/fnins.2015.00431

680 Schmidt PH, Dransfield DT, Claudio JO, Hawley RG, Trotter KW, Milgram SL,et al.
681 AKAP350, a multiply spliced protein kinase A-anchoring protein associated with
682 centrosomes. J Biol Chem. 1999; 274:3055-66. DOI: 10.1074/jbc.274.5.3055

683 Serrador JM, Cabrero JR, Sancho D, Mittelbrunn, M, Urzainqui A, Sánchez-Madrid F,
684 2004 HDAC6 Deacetylase Activity Links the Tubulin Cytoskeleton with Immune
685 Synapse Organization. Immunity, 20, 417–428. DOI: 10.1016/s1074-7613(04)00078-0

686 Sillibourne JE, Milne DM, Takahashi M, Ono Y, Meek DW. Centrosomal anchoring of
687 the protein kinase CK1delta mediated by attachment to the large, coiled-coil scaffolding

688 protein CG-NAP/AKAP450. J Mol Biol. (2002) 322:785–97. DOI: 10.1016/S0022-
689 2836(02)00857-4.

690 Takahashi M, Yamagiwa A, Nishimura T, Mukai H, Ono Y. Centrosomal Proteins CG-
691 NAP and Kendrin Provide Microtubule Nucleation Sites by Anchoring γ-Tubulin Ring
692 Complex. Mol Biol Cell. 2002; 13: 3235–3245. DOI: 10.1091/mbc.E02-02-0112

693 Tian L, Nelson DL, Stewart, DM. Cdc42-interacting protein 4 mediates binding of the
694 Wiskott-Aldrich syndrome protein to microtubules. *J. Biol. Chem*. 2000; 275:7854-7861.
695 DOI: 10.1074/jbc.275.11.7854

696 Tonucci FM, Almada E, Borini-Etichetti C, Pariani A, Hidalgo F, Rico MJ, Girardini J,
697 Favre C, Goldenring JR, Menacho-Marquez M, Larocca MC. Identification of a CIP4
698 PKA phosphorylation site involved in the regulation of cancer cell invasiveness and
699 metastasis. Cancer Lett. 2019; 461:65-77. DOI: 10.1016/j.canlet.2019.07.006.

700 Tonucci FM, Ferretti A, Almada E, Cribb P, Vena R, Hidalgo F, Favre C, Tyska MJ,
701 Kaverina I, Larocca MC. Microtubules regulate brush border formation. J Cell Physiol.
702 2018; 233:1468-1480. DOI: 10.1002/jcp.26033.

703 Tonucci FM, Hidalgo F, Ferretti A, Almada E, Favre C, Goldenring JR, Kaverina I,
704 Kierbel A, Larocca MC. Centrosomal AKAP350 and CIP4 act in concert to define the
705 polarized localization of the centrosome and Golgi in migratory cells. J Cell Sci. 2015;
706 128:3277-89. DOI: 10.1242/jcs.170878.

707 Tsujita K, Suetsugu S, Sasaki N, Furutani M, Oikawa T, Takenawa T. Coordination
708 between the actin cytoskeleton and membrane deformation by a novel membrane
709 tubulation domain of PCH proteins is involved in endocytosis. J. Cell Biol. 2006;
710 172:269-279. DOI: 10.1083/jcb.200508091

711 Zilberman, Y., Ballestrem, C., Carramusa, L., Mazitschek, R., Khochbin, S., and
712 Bershadsky, A. Regulation of microtubule dynamics by inhibition of the tubulin
713 deacetylase HDAC6. J Cell Sci 2009; 122, 3531–3541. DOI: 10.1242/jcs.046813

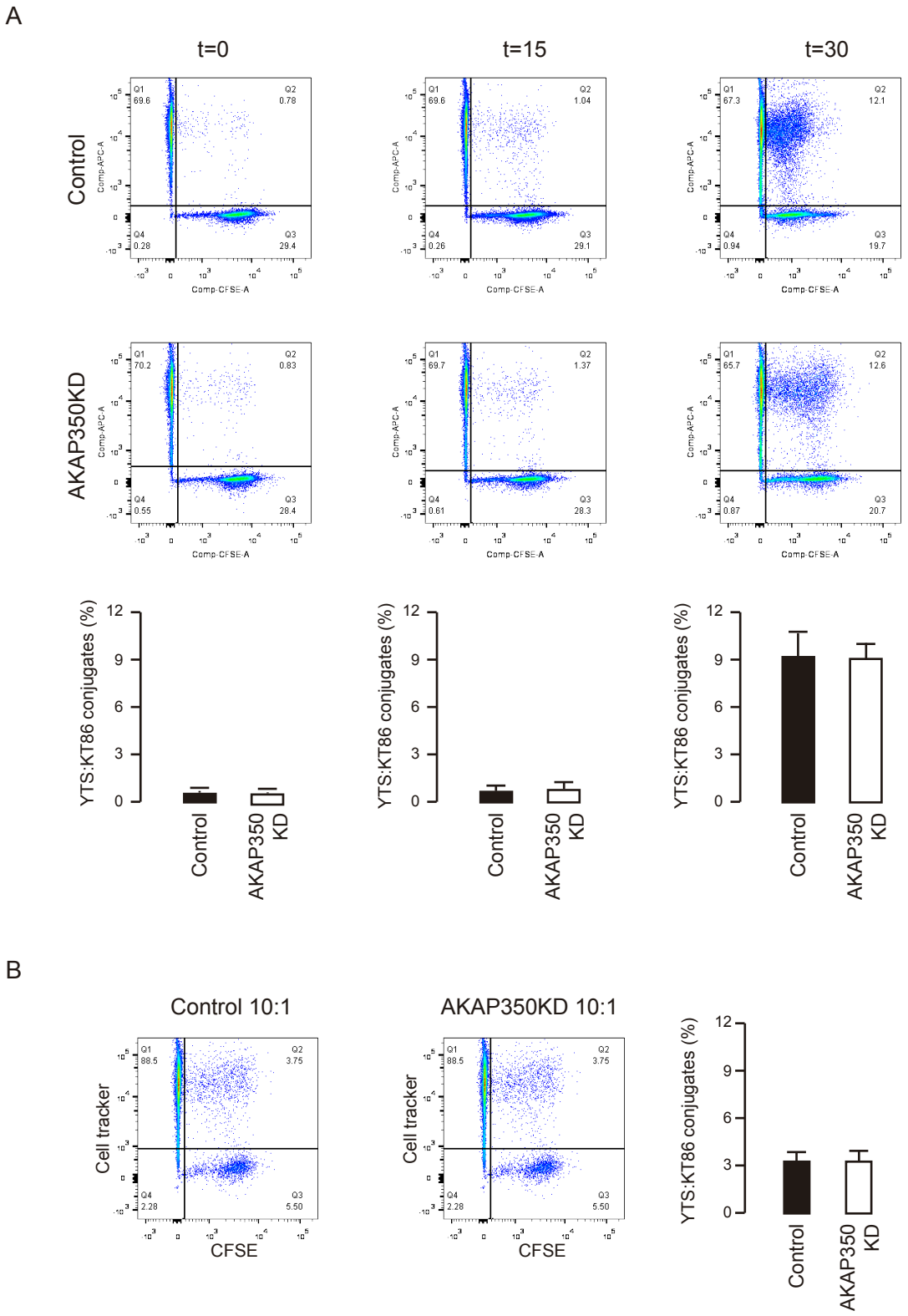

Supplementary figure 1. Reduction of AKAP350 expression does not affect YTS:KT86 conjugate formation. YTS control and AKAP350KD cells were stained with cell tracker Deep red and mixed with KT86 cells stained with CFSE. Conjugate formation was analyzed by flow cytometry. The conjugates were determined as CFSE/cell tracker Deep red double positive events. Effector and target cells were mixed at a 2:1 (A) or 10:1 (B) ratio and incubated at 37 °C and 5 % CO2 for the indicated periods (A) or for 30 min (B). Bars represent the mean percentage of conjugates formation from three independent experiments. Error bars represent SEM. *p< 0.05.

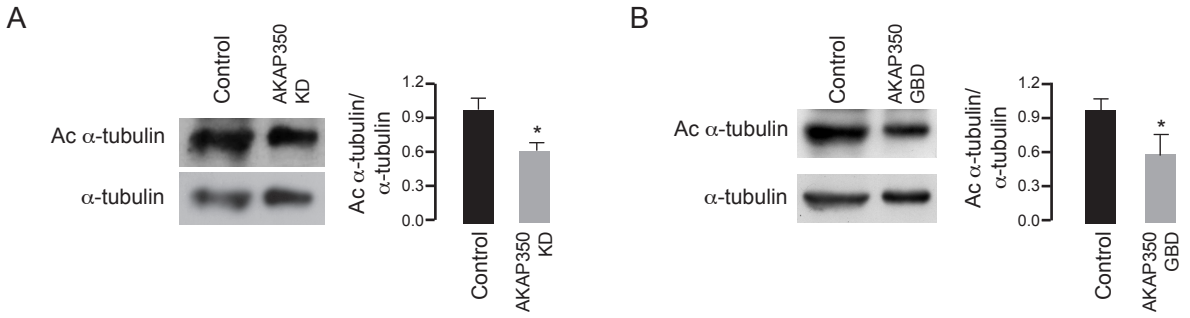

Supplementary figure 2. AKAP350 expression and localization at the Golgi apparatus is required for proper microtubule acetylation. Acetylated α-tubulin and total α-tubulin levels in control, AKAP350KD (A) and AKAPGBD (B) cell lysates were analyzed by WB. The bars chart represents the mean density of the band corresponding to acetylated α-tubulin relative to α-tubulin for three independent experiments. Error bars represent SEM. *$p < 0.05$.